ELSEVIER

Interactions of Particles and Microbubbles with Turbulence

M. R. Maxey
E. J. Chang*
Center for Fluid Mechanics, Turbulence and Computation, Brown University, Providence, Rhode Island

L-P. Wang
Department of Mechanical Engineering, Pennsylvania State University, University Park, Pennsylvania

■ Dilute, dispersed two-phase flows arise in many contexts ranging from solid particles or droplets in gas flows to bubbles in liquids. Many of the flows of interest are turbulent, which presents a complex problem to analyze or to determine the dominant physical processes contributing to the observed phenomena. Advances in experimental techniques have made it possible to measure directly turbulent and particle velocity fluctuations in dilute systems. This has provided a counterpart to advances in computational and analytical models and a basis on which to test these models. Three specific areas are considered: the fluctuating forces on an individual particle in an unsteady flow, the response of a solid particle to a turbulent air flow, and the corresponding response of a small bubble in turbulent liquid flows. Results from direct numerical simulations are presented for each of these, including the nonuniform distribution of particles generated by local instantaneous features of the flow. The issue of turbulence modulation at low to moderate void fractions is discussed.

Keywords: *turbulent flows, turbulence modulation, particle–microbubble interaction, dilute two-phase systems*

INTRODUCTION

The study of two-phase flows has developed in many different directions due to the varied contexts in which they appear. The transport of solid particles or liquid droplets in a gas flow, for example, is studied by mechanical engineers for the combustion of pulverized coal or fuel sprays, while atmospheric scientists are concerned with similar issues for rain formation in clouds or the persistence of volcanic ash in the atmosphere following an eruption. Solid particles in liquids arise in the transport of solids in slurries, in sedimentation in estuaries and rivers, and in chemical reactor processes. Bubbles in liquids are of concern for nuclear reactor safety, oil well measurements, hydroelectric power systems, cavitation, and underwater acoustics. Despite the variety of contexts, these systems share a number of common aspects and may be classified accordingly. One such classification is whether the flows are dilute, dispersed two-phase flows with low-volume void fraction or whether the particles are more densely packed as in a fluidized bed. The focus of this paper is on dilute systems, at low void fraction, in which the individual particles or bubbles are well separated.

The development of theoretical models for adiabatic two-phase flow has been strongly influenced by the type of experimental measurements that have been possible. In flows where the volume void fraction is large, around 10% or more, there are strong complex dynamical interactions between the phases. Optical techniques are limited to visual observations of flow quality and classification into specific flow regimes. Measurements have focused on overall average quantities such as the mean pressure drop along the length of a pipe or the mean void fraction. Conductivity sensors or impedance probes are used to measure void fractions, and wall-mounted pressure sensors to obtain pressure drops. For bubbly, gas–liquid flows in vertical or horizontal tubes, these observations form the basis for flow regime diagrams such as the Mandhane [1] diagram. These delineate the stability of, say, annular flow from dispersed bubble flow in terms of the equivalent mean volume flow rate or superficial velocity of each phase. Spedding and Spence [2] present a recent review of results in this area. A more fundamental description for these high void fraction, bubbly flows is the drift-flux model, which relates liquid flow rates and added-mass effects of the bubbles. A good summary of this approach with some new results is given by Kowe et al. [3]. Experimental methods in general for two-phase flows, especially those suited to large void fraction, are surveyed by Snoek

Address correspondence to Dr. Martin R. Maxey, Center for Fluid Mechanics, Turbulence and Computation, Box 1966, Brown University, Providence, RI 02912.

Experimental Thermal and Fluid Science 1996; 12:417–425

655 Avenue of the Americas, New York, NY 10010

0894-1777/96/$15.00
SSDI 0894-1777(95)00130-1

*Present address: Naval Research Laboratory, Code 6410, Washington, DC 20375.

[4]. However, it would appear that even with recent advances in experimental methods, our understanding of gas–liquid flows under these conditions will remain limited to determining bulk flow quantities for some time to come.

At low void fractions in dispersed two-phase flow, other, more detailed measurements are possible and a wider range of experimental techniques can be applied. The ability to obtain measurements of turbulent velocity fluctuations in the fluid phase and velocities of the individual particles or bubbles has greatly increased understanding in this area and prompted more detailed theoretical analysis. The influence of small solid particles in a turbulent air flow has been studied by Tsuji et al. [5] using laser-Doppler velocimetry (LDV). First the air flow was seeded with small tracer smoke particles to give the flow velocity data; then larger polystyrene particles were introduced as the particle phase. Signal discrimination methods were applied to separate the velocity signals for the air flow and those for the particle phase. Typical density ratios of particles to air of 1000 : 1 mean that even at very low void fractions significant turbulence modification may occur. The low void fraction is essential to the feasibility of the LDA measurements and minimal interference with the optical beams. Similar LDA methods have been employed for gas–solid flows by Wells and Stock [6] and Longmire and Eaton [7] for measurements of particle dispersion in homogeneous turbulence and jet flows, respectively.

Flows containing small bubbles, even in dilute dispersed systems, present extra difficulties because the volume void fractions of interest are generally higher, typically a few percent. LDA techniques have been successfully employed by Theofanous and Sullivan [8] and Lance and Bataille [9] even in this context when special precautions were taken to minimize optical path interference. Successful measurements even at void fractions close to 7% have been reported [9]. Bonetto and Lahey [10], in recent work on air entrainment by plunging jets, have shown how LDA methods can be employed to obtain instantaneous measurements not only of bubble velocities, but also of bubble size and volume void fraction. Particle image velocimetry (PIV) has proven to be a valuable technique also, and by tracking the motion of both bubbles and tracer particles from photographic images it is possible to obtain simultaneous data on bubble velocity and local flow conditions [11]. Ran and Katz [12] have also proposed a technique whereby recorded images of changing sizes of microbubbles may be used to infer local variations in the fluid pressure field. The developments in experimental methods have motivated new developments in analysis and computation.

An aim of this paper is to present some results on the computation of particle and bubble interactions with turbulence. Two approaches have developed in the analysis of dilute two-phase flows. One is the use of continuum, two-fluid models [13] whereby the fluid phase and the particle or bubble phase are considered separately. Continuum equations for mass conservation and momentum are formulated for each phase, with an indicator function $\chi(\mathbf{x}, t)$ used to indicate where a point $\mathbf{x}$ in the flow lies instantaneously in the fluid phase ($\chi = 1$) or in the particle phase ($\chi = 0$). In any two-phase flow there is a random distribution of particles through either the initial distribution of the particles or random turbulent mixing or both. The mean volume void fraction at any point then corresponds to the ensemble mean value $\langle(1 - \chi)\rangle$. Continuum models are based on such ensemble averages to give continuous field variables, and where such flows are turbulent they usually involve turbulence closure assumptions. A key component of such models is the specification of the momentum transfer between the phases, which comes down to specifying correctly the fluctuating fluid force that acts on a particle and the corresponding reaction force of the particle on the fluid. Versions of these models have been used to study flow stability—by Saffman [14] for dusty gas flows in plane Poiseuille flow and by Yang et al. [15] for gas–solid wake flows.

A second approach that has been developed is the direct numerical simulation of dilute particle-laden flows. Here the equations of fluid motion are specified and solved directly by numerical computation. A large, but finite, number of particles are included, and the trajectory of each particle is computed from its own equation of motion and a specification of the instantaneous fluid force acting on it determined from the local flow conditions. In very dilute systems there is no significant dynamical feedback on the flow from the particles, and they respond passively to the flow. Simulations such as these avoid the issue of closure assumptions and provide results on particle mixing in transitional [16, 17] or turbulent [18, 19] flow. Dynamical coupling can be represented by applying a body force to the fluid motion where the force is the cumulative effect of the reaction forces from the individual particles. For example, Squires and Eaton [20] have pursued this approach in studying the degree of flow modification in homogeneous turbulence. A somewhat different but comparable approach has been developed by Sangani et al. [21] to investigate bubbly liquids subject to small-amplitude oscillations.

In the following sections we present some computational results for a number of topics that we have studied recently. These include the forces acting on small particles in unsteady flow, the turbulent mixing of solid particles in gas flows, and the distribution of small microbubbles in liquid flows.. These are a personal selection from a wide range of possible topics in two-phase flow. We conclude with some comments on turbulence modulation and outstanding experimental issues.

FORCES ON A PARTICLE

As we noted above, an essential step in formulating two-phase continuum models or the direct numerical simulation of particle trajectories in a turbulent flow is to specify correctly the fluid forces acting on a particle. These forces will depend on the velocity of the particle and the local flow conditions. A spherical particle is the simplest to consider and is a good representation for small liquid droplets in air or microbubbles in water where surface tension is sufficient to maintain the spherical shape, typically for diameters less than 1 mm. If the particle is smaller than the scale on which the ambient flow varies, the Kolmogorov scale in turbulent flow, and the Reynolds number for the motion relative to the surrounding fluid is

small, then these forces can be found from the theory of unsteady Stokes flow. The resulting equation of particle motion is given by Maxey and Riley [22] as

$$m_p \frac{d\mathbf{V}}{dt} = (m_p - m_F)\mathbf{g} + m_F \frac{D\mathbf{u}}{dt} - \frac{1}{2} m_F \frac{d}{dt}\left[\mathbf{V} - \mathbf{u}(\mathbf{Y}(t), t) - \frac{a^2}{10}\nabla^2 \mathbf{u}\right] - 6\pi a \mu \mathbf{H}(t) - 6\pi a^2 \mu \times \int_0^t \frac{d\mathbf{H}}{d\tau}[\pi\nu(t-\tau)]^{-1/2}\, d\tau. \quad (1)$$

See also Gatignol [23] and Maxey [24]. In this equation m_p denotes the mass of the spherical particle, which has radius a, and m_F denotes the equivalent mass of the displaced fluid. The acceleration due to gravity is $\mathbf{g}$, the dynamic and kinematic fluid viscosities are μ and ν, respectively. The position of the sphere center is $\mathbf{Y}$ and moves at velocity $\mathbf{V}$ through an ambient flow $\mathbf{u}(\mathbf{x}, t)$. The quantity $\mathbf{H}(t)$ is determined by the relative motion,

$$\mathbf{H}(t) = \mathbf{V}(t) - \mathbf{u}(\mathbf{Y}(t), t) - \frac{1}{6}a^2 \nabla^2 \mathbf{u}, \quad (2)$$

where the Laplacian is evaluated at $x = \mathbf{Y}(t)$. The form of the integral requires $\mathbf{H}(0) = 0$ as an initial condition.

The first term on the right in Eq. (1) represents the weight of the particle and possible buoyancy forces, while the second is the fluid force from the undisturbed flow, without the particle present, that would act on the equivalent fluid mass. The third term is due to added-mass effects, with the usual coefficient of $1/2$, and is modified to take account of spatial variations in the flow. The last two terms are the steady Stokes drag force and the Basset history term, again modified to account for possible velocity gradients in the flow. This history term is the result of the finite time scale for vorticity to diffuse from the sphere as it accelerates. These estimates assume that the Reynolds numbers

$$\mathrm{Re} = 2aW/\nu \quad (3)$$

and

$$\mathrm{Re}_\beta = 2a^2\beta/\nu \quad (4)$$

are both small, where W is a scale for the slip velocity $\mathbf{u} - \mathbf{V}$ and β is a scale for the fluid velocity gradient $\nabla\mathbf{u}$. Equation (1) provides a good estimate for solid spheres, for liquid droplets due to the usually large ratio of the liquid- to gas-phases viscosities, and for small bubbles due to the effect of surfactants. Unless special precautions are taken, surfactants present in water will quickly coat the surface of a microbubble and "freeze" the surface, giving an effectively rigid particle response [25]. A microbubble 100 μm in diameter in water will typically rise at a terminal speed of $1/2$ cm/s in still fluid [26].

As particle size increases, the Reynolds numbers increase and other factors must be considered. One of these is the form of the added-mass effect. In deriving Eq. (1), the time derivative following a particle is used for the added mass. A more accurate form [27] is

$$\frac{1}{2} m_F \left(\frac{d\mathbf{V}}{dt} - \frac{D\mathbf{u}}{Dt}\right), \quad (5)$$

at least when the ambient flow $\mathbf{u}$ is inviscid. At low Reynolds numbers form (5) and that used in Eq. (1) are not formally distinguishable. Direct numerical simulations by Rivero et al. [28] support this modified form for finite Reynolds numbers. Another feature is the generation of lift forces due to particle rotation [29] or shear velocity gradients [30]; these forces are not found under Stokes flow conditions. Improved estimates have been made by McLaughlin [31] for the lift force in a shear flow at low but finite Reynolds numbers for rigid particles, and some numerical results have been given by Dandy and Dwyer [32].

Other issues include the appropriate form of the drag force on a sphere at finite Reynolds numbers in unsteady flows and whether or not the added-mass coefficient remains $1/2$. As part of a continuing study into these issues, Chang [33] conducted a series of direct numerical simulations for unsteady flow past a fixed rigid sphere. The ambient flow is unidirectional,

$$\mathbf{u}(\mathbf{x}, t) = U(t)\hat{\mathbf{e}}, \quad (6)$$

where $\hat{\mathbf{e}}$ is a fixed unit vector. The resulting flow is axisymmetric, with $\hat{\mathbf{e}}$ as the symmetry axis. The equations for viscous, incompressible flow are solved by a spectral method based on a Fourier representation in the polar angle θ and a Chebyshev polynomial expansion in the radial coordinate r. A vorticity–stream function formulation was used to ensure that incompressible flow conditions were satisfied and to avoid the need for pressure boundary conditions. The numerical procedures are summarized in [34]. From the simulation data, flow structure and forces on the sphere can be investigated.

We first present results for an oscillatory flow $U(t) = -U_0 \sin(\sigma t)$ obtained for a nondimensional frequency $S_t = \sigma a/U_0$ of 0.625 and a peak Reynolds number $\mathrm{Re} = 2aU_0/\nu$ of 16.73. These values correspond to an experiment done by Odar [35] for which data are available. Figure 1 shows a time sequence of the streamlines in the flow as it proceeds from peak freestream flow at a phase angle $\sigma t = \pi/2$ to flow reversal at $\sigma t = \pi$. A clear feature is the flow separation that occurs on the decelerating phase with a detached eddy at flow reversal, while a new layer of vorticity forms at the surface. Under steady conditions, flow separation does not arise until Re exceeds 20 and even then results in a much smaller separation bubble. Figure 2 shows a corresponding variation in the computed drag force, with a comparison with Odar's experiments and the Basset estimate for unsteady Stokes flow, Eq. (1). The experimental data have some irregularities close to flow reversal due to the experimental setup. Generally the correspondence is good. Odar and Hamilton [36], among others, have proposed modifications to Eq. (1) for finite Reynolds numbers and locally uniform flow. These are based on introducing empirical coefficients for the added-mass and history terms that depend on an acceleration parameter but not the Reynolds number, while the Stokes drag is replaced by the nonlinear drag that would act under steady flow conditions at the same instantaneous value of the Reynolds number. This

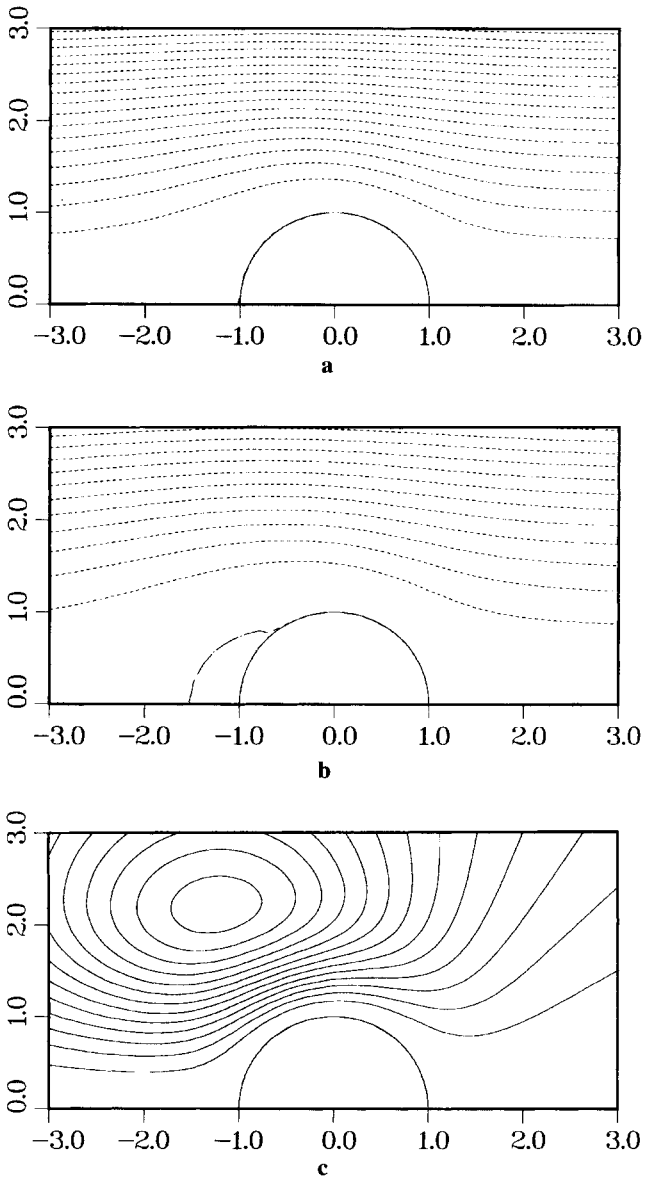

Figure 1. Sequence of streamline patterns (from top) at $\sigma t = \pi/2, 3\pi/4, \pi$ for oscillatory flow, Re = 16.73 and $S_t = 0.625$. Sphere, $a = 1$, shown.

estimate is shown too. It is clear that in this instance there is little to choose between them.

Other results were obtained for a flow that decelerated at a constant rate. The value of *Re* was initially 10 and decreased linearly to a value of 5 over a nondimensional time interval $\Delta t\, U_0/a = 1/2$ as the free-stream velocity dropped from U_0 to $(1/2)U_0$. The initial flow was fully developed steady flow. The advantage of this flow change, as reported by Rivero et al. [28], is that it is possible to clearly identify the added-mass contribution. Figure 3 shows the instantaneous forces on the sphere due to the pressure distribution C_P and the viscous shear stress C_F. Both are scaled by $\rho\pi a^2 U_0^2$, where ρ is the fluid density, and the value C_D is the resultant force $(C_P + C_F)$. Immediately after the deceleration is applied or removed there is a jump in the pressure force C_P. The magnitude of the

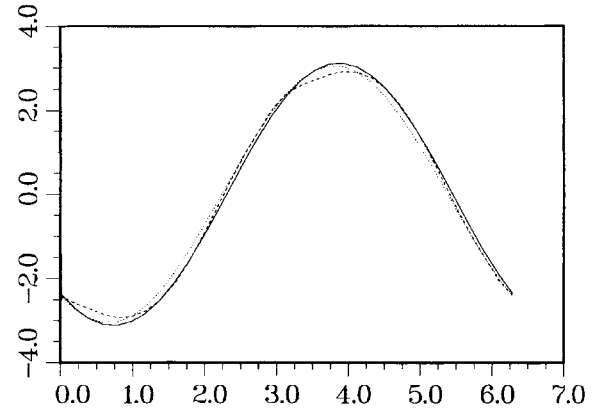

Figure 2. Resultant drag force C_D during oscillation cycle (——) simulation; (---) Basset; (-·-) Odar.

jump is exactly matched to that for an added-mass coefficient of 1/2. Somewhat surprisingly, the force C_F due to viscous shear stresses reverses even though the flow is still in forward motion. A plot of the vorticity in the flow, Fig. 4, at the time when $C_F = 0$ shows clearly that separation has occurred. Near the surface of the sphere the local flow is reversed over a substantial portion of the surface, leading to the net negative value of C_F.

These results illustrate that even at modest Reynolds numbers the flow structure around a sphere can be quite varied, and it will be a while yet before we can say for certain what the appropriate extension of Eq. (1) should be for higher Reynolds numbers. For several applications Eq. (1) may be quite adequate in practice even though not justified in theory. The issue of lift forces needs to be addressed further.

SOLIDS IN GAS FLOWS

A solid spherical particle (or droplet) in a gas flow has a much larger density so that terms in m_F in Eq. (1) may be neglected. Further the history term will generally be small, except for possible initial transients to the motion, if the particle size is small enough. For example, if τ_0 is a time scale for the particle acceleration in response to changes in the flow conditions, then one would require $a/(\nu\tau_0)^{1/2}$

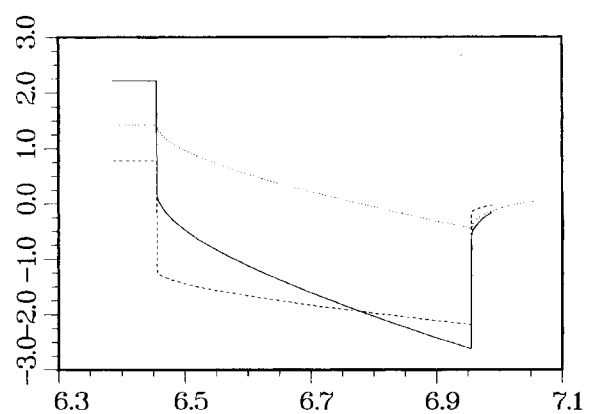

Figure 3. Forces on sphere in decelerating flow. (-·-) C_P; (---) C_F; (——) C_D.

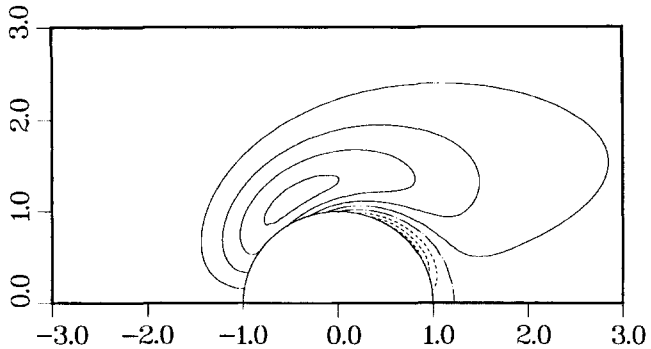

Figure 4. Vorticity contour plot for flow at end of deceleration interval.

to be small. In a turbulent flow the shortest time scale on which the flow changes is τ_K, the Kolmogorov time scale,

$$\tau_K = (\nu/\epsilon)^{1/2}, \tag{7}$$

ϵ being the rate of kinetic energy dissipation per unit mass in the flow. Thus if $\tau_0 = \tau_K$, the condition is equivalent to the particle size being small compared to the Kolmorgorov length scale η, where

$$\eta = (\nu^3/\epsilon)^{1/4}. \tag{8}$$

The Kolmogorov velocity scale v_κ is equal to η/τ_K and is representative of velocity fluctuations in the small-scale dissipation range of the turbulence. The dominant factors governing particle motion are particle inertia, viscous drag forces, and the particle weight. Within the Stokes range, Re < 1, the motion of a single isolated particle can be determined from

$$\frac{d\mathbf{V}}{dt} = \frac{\mathbf{u}(\mathbf{Y},t) - \mathbf{V}(t) + \mathbf{W}^{(s)}}{\tau_P}, \tag{9}$$

where $\mathbf{W}^{(s)}$ is the Stokes velocity, the terminal fall speed in still fluid,

$$\mathbf{W}^{(s)} = m_P\mathbf{g}/6\pi a\mu, \tag{10}$$

and τ_P is the inertial response time of the particle,

$$\tau_P = m_P/6\pi a\mu. \tag{11}$$

Even for very small solid particles τ_P can be significant in a gas flow.

The usual focus of attention in the study of dilute gas–solid flows has been the turbulent dispersion of the particles [6, 16–19]. Theoretical estimates for the effects of varying τ_P on the long-term dispersion have been given by Reeks [37] among others. The effect of particle settling, $W^{(s)}$, gives rise to the crossing-trajectories effect [38], which reduces particle dispersion compared to that of Lagrangian fluid elements, as has been demonstrated by the experiments of Wells and Stock [6]. Dispersion is governed by the large eddies in a turbulent flow. The effects of varying $W^{(s)}$ or τ_P are classified by scaling these with the rms velocity fluctuation u' or the large-eddy turnover time $T_E = L/u'$, where L is the integral length scale, as in the numerical simulations of Squires and Eaton [18]. A similar viewpoint is taken by Gore and Crowe [39, 40] for flows where the mass loading is sufficient to cause modification of the turbulence.

Recent studies by Wang and Maxey [41] have demonstrated that particle–turbulence interactions can be significant for much smaller particles, when $\tau_P/\tau_K = O(1)$. Direct numerical simulations of homogeneous, isotropic turbulence were performed using spectral Fourier representations for the flow and periodic boundary conditions. A forcing scheme applied to the low-wavenumber Fourier modes ensured that a statistically stationary turbulent flow could be maintained. Simulations were performed at Reynolds numbers Re_λ, based on u' and the Taylor microscale λ, ranging from 31 on a 48^3 grid to 62 on a 96^3 grid. The motion of each particle was computed by solving Eq. (9) at each time step.

When τ_P is much shorter than τ_K, the particle responds to all frequencies in the turbulent flow and moves at every instant at a velocity

$$\mathbf{V}(t) = \mathbf{u}(\mathbf{Y}(t),t) + \mathbf{W}^{(s)}, \tag{12}$$

so that the right-hand side of Eq. (9) is zero. Results for the mean particle settling velocity in homogeneous turbulence, with zero mean flow, are exactly the same as in still fluid [42]. However, as τ_P becomes larger, inertial effects come into play, at least for the fine-scale dissipation range turbulence characterized by Kolmogorov scales. This is illustrated by Fig. 5, which shows the change in mean particle settling velocity as τ_P/τ_K is varied. The greatest change occurs when $\tau_P/\tau_K = O(1)$. Unlike dispersion, the settling rate is more strongly influenced by interactions with small-scale turbulence.

For small particles where the particle inertia has only a weak effect, Eq. (12) may be used as a first estimate of the particle velocity $\mathbf{V}(t)$ and substituted back into Eq. (9) to obtain a first approximation for inertial effects. This yields [42]

$$\mathbf{V}(t) = \mathbf{u}(\mathbf{Y}(t),t) + \mathbf{W}^{(s)} - \tau_P\left(\frac{\partial\mathbf{u}}{\partial t} + [\mathbf{u} + \mathbf{W}^{(s)}]\cdot\nabla\mathbf{u}\right), \tag{13}$$

with all quantities evaluated at $\mathbf{x} = \mathbf{Y}(t)$. This defines a "particle flow field" that is determined solely by the instantaneous particle position, and this flow field is compressible,

$$\nabla\cdot\mathbf{V} = -\tau_P\nabla\cdot(\mathbf{u}\cdot\nabla\mathbf{u}). \tag{14}$$

Further simplification of Eq. (13) reveals that particles will be "compressed" or biased toward regions of instantaneously high strain rate or low vorticity or both. This bias mechanism was shown [42] to be the cause of the change

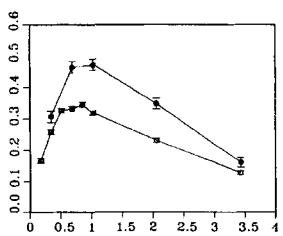

Figure 5. Increase in mean settling rate ($\langle\mathbf{V}\rangle - \mathbf{W}^{(s)}$), scaled by v_K against ratio τ_P/τ_K for $W^{(s)} = v_K$. (○) $\mathrm{Re}_\lambda = 31$; (●) $\mathrm{Re}_\lambda = 62$. Error bars indicated.

in mean settling rate. It has been observed in numerical simulations of turbulence for nonsettling particles [18] and settling particles [41]. As an illustration, Fig. 6 shows the particle distribution in a planar section from a turbulent flow computation at a single instant. The corresponding vorticity distribution is also shown. Figure 7 shows more specifically the local particle number density, conditionally sampled and averaged in turn on the value of the vorticity magnitude Ω and the magnitude of the rate of strain S. Instantaneously, $2\nu S^2$ is the viscous dissipation rate at a point in the turbulence. The correlation of particle concentration with rate of strain is clearly visible.

It would appear that significant particle–turbulence interactions may occur even when $\tau_P \sim \tau_K$ and yet $\tau_P \ll T_E$. Small eddies within the dissipation range contribute most to the vorticity and rate of strain distributions, so the bias mechanism will be most obvious at these scales. When τ_P substantially exceeds τ_K, the particles are less sensitive to the small-eddy motions, and local accumulations in a turbulent flow will be controlled more by the vorticity in the large eddies. Experiments so far have not confirmed these effects. The increase in settling velocities would be relevant to, say, small droplets of 20–50 μm diameter in air, but nonlinear drag effects will limit this increase if Re > 1. The accumulation effect should be measurable in either context.

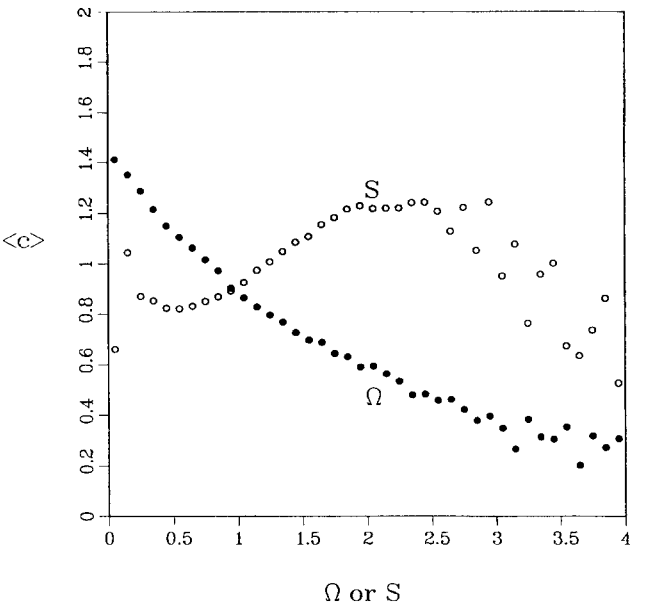

Figure 7. Conditionally averaged particle concentration against vorticity Ω and rate of strain S, scaled by rms values. (○) S; (●) Ω. $\tau_P/\tau_K = 1$, $W^{(s)} = v_K$, $\mathrm{Re}_\lambda = 31$.

MICROBUBBLES IN WATER

As noted earlier, microbubbles less than 1 mm in diameter respond as rigid spherical particles, at least as an initial approximation. For Re < 1, Eq. (1) may be used to determine the motion of an individual microbubble in a turbulent flow at low void fraction. The bubble has essentially no mass, $m_P = 0$, and the inertial response is strongly influenced by added-mass effects. The smallest bubbles will respond fully to the turbulence at all time scales, and the velocity of a bubble $\mathbf{V}(t)$ will be given as in Eq. (12), where now $\mathbf{W}^{(s)}$ is the bubble rise velocity in still fluid. As bubble size increases to the point that an inertial response is significant, the particle Reynolds number Re also increases to $O(1)$. The details of the fluid forces become more critical for Re > 1, and more careful consideration of how Eq. (1) extends to flows for which Re > 1 is needed, including the way in which lift forces may be a factor [27]. A useful approximate equation of motion that includes the essential features is

$$0 = -m_F\mathbf{g} + m_F\frac{D\mathbf{u}}{Dt} - \frac{1}{2}m_F\left[\frac{d\mathbf{V}}{dt} - \frac{D\mathbf{u}}{Dt}\right] - 6\tau a\mu[\mathbf{V} - \mathbf{u}(\mathbf{Y}(t), t)], \tag{15}$$

which uses Eq. (5). This can be rewritten in terms of the bubble response time τ_B and terminal rise velocity $\mathbf{Q}$,

$$\tau_B = m_F/12\pi a\mu, \tag{16}$$

$$\mathbf{Q} = -m_F\mathbf{g}/6\pi a\mu, \tag{17}$$

$$\frac{d\mathbf{V}}{dt} = 3\frac{D\mathbf{u}}{Dt} - \frac{\mathbf{V}(t) - \mathbf{u}(\mathbf{Y}(t), t) - \mathbf{Q}}{\tau_B}. \tag{18}$$

Numerical simulations of microbubble motion, based on Eq. (18), in a turbulent flow were performed recently [43] in a manner similar to that for gas–solid flows described previously. A stationary isotropic homogeneous turbulent flow was maintained by forcing the large-scale motion while allowing the small-scale dissipation scales to evolve naturally. Again a strong interaction was found with the small-scale turbulence when $\tau_B \sim \tau_K$, with locally very strong concentrations of the microbubbles. This time, though, the accumulations were correlated with regions of

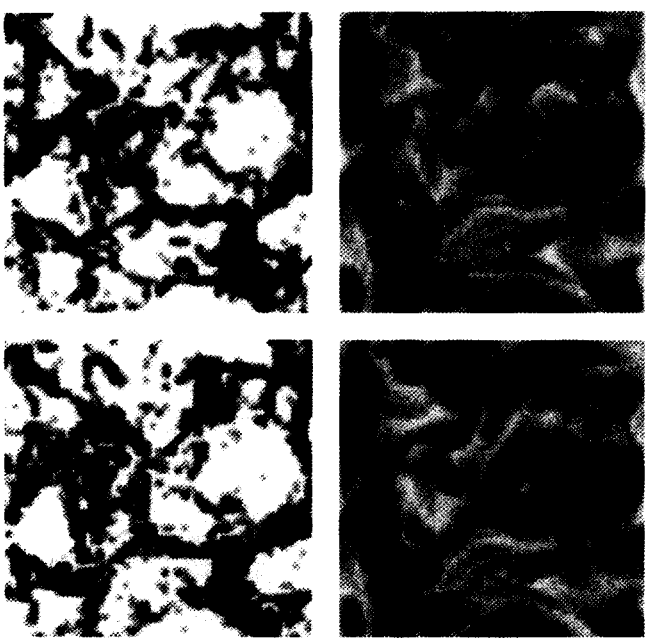

Figure 6. Relative particle concentration (left) and vorticity magnitude Ω (right) in a vertical section of the flow, $\mathrm{Re}_\lambda = 31$. $\Omega = 0$ white; $\Omega \geq 2$, black; Ω scaled by rms value.

strong vorticity or low strain rate. Figure 8 shows results for $Re_\lambda = 31$.

This change in the bias may be understood by an approximation similar to Eqs. (12) and (13) but based now on Eq. (18) for small values of τ_B. The "bubble flow field" is compressible, and

$$\nabla \cdot \mathbf{V} = 2\tau_B \nabla \cdot (\mathbf{u} \cdot \nabla \mathbf{u}), \tag{19}$$

which is the opposite of Eq. (14). Thus bubbles accumulate in regions of stronger vorticity and would naturally spiral in toward a vortex core whereas a Lagrangian fluid element would follow a closed circular streamline in a steady flow. What is surprising is the degree to which bubble accumulation occurs in a turbulent flow that is changing rapidly at small scales. The turbulence also reduces the mean bubble rise velocity even in the absence of a mean flow. Typically, for $Q = v_K$ a net reduction of 25–50% in the mean rise velocity occurs as τ_B/τ_K varies between 0 and 2.

TURBULENCE MODULATION

The results in the previous sections have been based on the motion of individual particles in isolation from each other. No dynamical coupling of the particle phase back on the turbulent flow has been included. Nevertheless the general patterns of particle or bubble accumulation in response to instantaneous flow conditions will persist in a fully coupled system, though these may be limited by the feedback of the particle dynamics on the flow.

There is not space in this short paper to discuss the present state of knowledge of turbulence modulation in dilute two-phase flow, nor it is our goal. Guidelines have been established by Gore and Crowe [39, 40] as to how turbulence levels may be affected by the presence of small particles. Experiments by Tsuji et al. [5] for solid particles in air flows and by Lance and Bataille [9] for bubbles in water both indicate that at low mass loading the particle phase enhances the overall dissipation of the flow, in general agreement with the simulation results of Squires and Eaton [20]. Viscous dissipation in the particle wakes, associated with the viscous drag force on the particles, is the most significant factor for small particles. Even "one-way coupled" simulations can be used to provide initial estimates of this and its spatial distribution [44, 45]. The local accumulation of particles can lead, for example, to quite strong local dissipation. Data on bubble or particle velocities obtained from experiments may be analyzed in the same way [46] to evaluate directly the local dissipation and the quantities used in turbulence models of two-phase flow.

OUTSTANDING ISSUES

Much remains to be answered about the mechanics of turbulence modulation, but advances in experimental methods are making it feasible to investigate details of the turbulence structure. There are, however, several immediate issues that could be answered by well-designed experiments. In our discussion of the settling of heavy particles in turbulent air flow a significant increase in mean settling velocity was found when τ_P and τ_K were comparable. This is a fairly robust observation from the numerical simulations, though the effect may be reduced for particle Reynolds numbers significantly larger than 1 due to the influence of the nonlinear drag. However, this increase in settling velocity has not been verified to date by experiments for homogeneous turbulence. In application to high

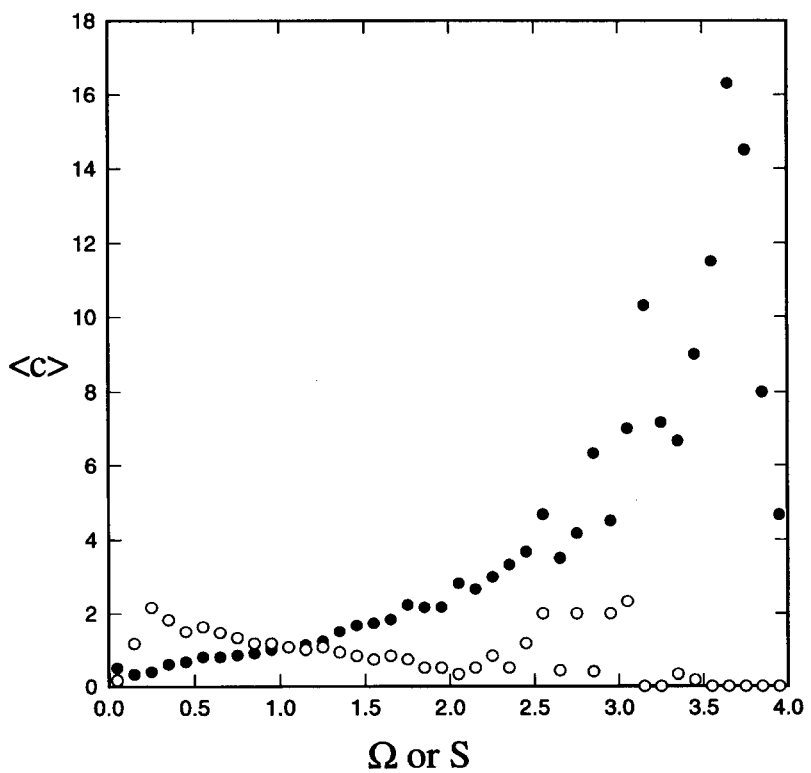

Figure 8. Same as Fig. 7 but for microbubble concentration, $\tau_B = \tau_K$, and $Q = v_K$.

Reynolds number turbulent flows, it is the small-scale, locally isotropic turbulence that will most significantly affect the mean settling velocity of small particles, while the large-scale structures in the flow will influence the dispersion most. The former can be characterized by the local value of the dissipation rate ϵ. Experiments by Lazaro and Lasheras [47, 48] have measured particle dispersion in free shear layers, for example, where there is a strong interaction with the large-scale structures. Dispersion of heavy particles in homogeneous turbulence has been studied by Wells and Stock [6]. In the latter an electrostatic potential was applied to deliberately increase the terminal fall velocity of each particle, but the issue of the turbulence affecting mean settling rates was not resolved.

An important practical issue in experiments is that the particles are not truly monodisperse but have a distribution of sizes. Thus it is not possible to decide independently whether or not a higher settling velocity is due to a larger particle size. What is required are simultaneous data on the particle vertical velocity and particle size within an observation region.

For small bubbles in turbulence, again there is no experimental verification of the reduction in mean rise velocity by the interaction with small-scale, locally homogeneous turbulence. This reduction should be larger than the corresponding increase for particles. Results from either experiment would be welcome and would assist in the development of reliable predictive models for particle and bubble transport.

We acknowledge the support by the Office of Naval Research, Fluid Mechanics Program (N00014-91-J-1340) and a DARPA U.R.I. award (N00014-86-K0754). The support of the Pittsburgh Supercomputing Center is also acknowledged.

NOMENCLATURE

a particle radius,
C_D fluid force on sphere, scaled by $\pi\rho a^2 U_0^2$,
C_F viscous shear force on sphere, scaled by $\pi\rho a^2 U_0^2$,
C_P pressure force on sphere, scaled by $\pi\rho a^2 U_0^2$,
$\hat{\mathbf{e}}$ unit vector, dimensionless
$\mathbf{g}$ constant of gravitational acceleration, cm/s^2
L integral length scale of turbulence,
m_F mass of fluid displaced by particle,
m_P mass of particle,
$\mathbf{Q}$ terminal rise velocity of bubble, Eq. (17),
r radial coordinate,
Re particle Reynolds number, Eq. (3), dimensionless
Re_β particle Reynolds number, Eq. (4), dimensionless
S magnitude of rate of strain
S_t frequency ($= \sigma a/U_0$), dimensionless
t time
T_E eddy turnover time scale, L/u',
$\mathbf{u}$ fluid velocity,
U free-stream velocity, Eq. (6),
u' rms turbulent velocity fluctuation
U_0 scale for free-stream velocity $U(t)$
v_K Kolmogorov velocity scale ($= \eta/\tau_K$),
$\mathbf{V}$ particle velocity, cm/s
W scale for slip velocity $\mathbf{u} - \mathbf{V}$, cm/s
$W^{(s)}$ Stokes terminal fall velocity, Eq. (10), cm/s
$\mathbf{x}$ position vector, cm
$\mathbf{Y}$ particle position, cm

Greek Symbols

β scale for fluid velocity gradient, s
Δt time interval for flow acceleration, s
ϵ rate of dissipation turbulent kinetic energy per unit mass, cm^2/s^3
η Kolmogorov length scale, Eq. (8), cm
θ angle coordinate, deg
μ dynamic viscosity of fluid, gm/(cm · s)
ν kinematic viscosity of fluid, cm^2/s
ρ fluid density, gm/cm^3
σ oscillation frequency, s^{-1}
τ_0 time scale of particle acceleration, s
τ_B bubble response time, Eq. (16), s
τ_K Kolmogorov time space, Eq. (7), s
τ_P particle response time, Eq. (11), s
Ω magnitude of fluid vorticity, s^{-1}

REFERENCES

1. Mandhane, J. M., Gregory, G. A., and Aziz, K., Flow Pattern Map for Gas–Liquid Flow in Horizontal Pipes, *Int. J. Multiphase Flow* **1**, 537–553, 1974.
2. Spedding, P. L., and Spence, D. R., Flow Regimes in Two-Phase Gas–Liquid Flow, *Int. J. Multiphase Flow* **19**, 245–280, 1993.
3. Kowe, R., Hunt, J. C. R. Hunt, A., Couet, B., and Bradbury, L. J. S., The Effects of Bubbles on the Volume Fluxes and the Pressure Gradients in Unsteady and Non-Uniform flows of Liquids, *Int. J. Multiphase Flow* **14**, 587–606, 1988.
4. Snoek, C. W., A Selection of New Developments in Multiphase Flow Measurement Techniques, *Exp. Thermal Fluid Sci.* **3**, 60–73, 1990.
5. Tsuji, Y., Morikawa, Y., and Shiomi, H., LDV Measurements of an Air–Solid Two-Phase Flow in a Vertical Pipe, *J. Fluid Mech.* **139**, 417–434, 1984.
6. Wells, M. R., and Stock, D. E., The Effects of Crossing Trajectories on the Dispersion of Small Particles in a Turbulent flow, *J. Fluid Mech.* **136**, 31–62, 1983.
7. Longmire, E. K., and Eaton, J. K., Structure of a Particle-Laden Round Jet, *J. Fluid Mech.* **236**, 217–257, 1992.
8. Theofanous, T. G., and Sullivan, J., Turbulence in Two-Phase Dispersed Flows, *J. Fluid Mech.* **116**, 343–362, 1982.
9. Lance, M., and Bataille, J., Turbulence in the Liquid Phase of a Uniform Bubbly Air–Water Flow, *J. Fluid Mech.* **222**, 95–118, 1991.
10. Bonetto, F., and Lahey, R. T., Jr., An Experimental Study on Air Carryunder Due to a Plunging Liquid Jet, *Int. J. Multiphase Flow* **19**, 281–294, 1993.
11. Adrian, R. J., Particle Imaging Techniques for Experimental Fluid Mechanics, *Annu. Rev. Fluid Mech.* **23**, 261–304, 1991.
12. Ran, B., and Katz, J., The Response of Microscopic Bubbles to Sudden Changes in the Ambient Pressure, *J. Fluid Mech.* **224**, 91–115, 1991.
13. Drew, D. A., Mathematical Modeling of Two-Phase Flow, *Annu. Rev. Fluid Mech.* **15**, 261–291, 1983.
14. Saffman, P. G., On the Stability of Laminar Flow of a Dusty Gas, *J. Fluid Mech.* **12**, 120–128, 1962.

15. Yang, Y., Chung, J. N., Troutt, T. R., and Crowe, C. T., The Effects of Particles on the Stability of a Two-Phase Wake Flow, *Int. J. Multiphase Flow* **19**, 137–149, 1993.
16. Crowe, C. T., Chung, J. N., and Troutt, T. R., Particle Mixing in Free Shear Flows, *Prog. Energy Combust. Sci.* **14**, 171–194, 1988.
17. Chung, J. N., and Troutt, T. R., Simulation of Particle Dispersion in an Axisymmetric Jet, *J. Fluid Mech.* **186**, 199–222, 1988.
18. Squires, K. D., and Eaton, J. K., Measurements of Particle Dispersion from Direct Numerical Simulations of Isotropic Turbulence, *J. Fluid Mech.* **226**, 1–35, 1991.
19. Elghobashi, S. E., and Truesdell, G. C., Direct Simulation of Particle Dispersion in Decaying Isotropic Turbulence, *J. Fluid Mech.* **242**, 655–700, 1992.
20. Squires, K. D., and Eaton, J. K., Particle Response and Turbulence Modification in Isotropic Turbulence, *Phys. Fluids* **A2**, 1191–1203, 1990.
21. Sangani, A. S., Zhang, D. Z., and Prosperetti, A., The Added Mass, Basset and Viscous Drag Coefficients in Nondilute Bubbly Liquids Undergoing Small Amplitude Oscillatory Motion, *Phys. Fluids* **A3**, 2955–2970, 1991.
22. Maxey, M. R., and Riley, J. J., Equation of Motion for a Small Rigid Sphere in a Nonuniform Flow, *Phys. Fluids* **26**, 883–889, 1983.
23. Gatignol, R., The Faxen Formulae for a Rigid Particle in an Unsteady Non-uniform Stokes Flow, *J. Méc. Theor. Appl.* **1**, 143–160, 1983.
24. Maxey, M. R., The Equation of Motion for a Small Rigid Sphere in a Nonuniform or Unsteady Flow, Fifth Int. Symp. on Gas–Solid Flow, ASME Fluids Eng. Conf., Washington, DC, June 1993.
25. Clift, R., Grace, J. R., and Weber, M. E., *Bubbles, Drops, and Particles*, pp. 171–202, Academic, New York, 1978.
26. Detsch, R. M., Small Air Bubbles in Reagent Grade Water and Seawater 1. Rise Velocities of 20 to 1000 μm Diameter Bubbles, *J. Geophys. Res.* **96** (C5), 8901–8906, 1991.
27. Auton, T. R., Hunt, J. C. R., and Prudhomme, M., The Force Exerted on a Body of Inviscid Unsteady Non-uniform Rotational Flow, *J. Fluid Mech.* **197**, 241–257, 1988.
28. Rivero, M., Magnaudet, J., and Fabre, J., New Results on the Forces Exerted on a Spherical Body by an Accelerated Flow, *C. R. Acad. Sci. Paris*, **312** (Ser. II), 1499–1506, 1991.
29. Rubinow, S. I., and Keller, J. B., The Transverse Force on a Spinning Sphere Moving in a Viscous Fluid, *J. Fluid Mech.* **11**, 447–459, 1961.
30. Saffman, P. G., The Lift on a Small Sphere in a Slow Shear Flow, *J. Fluid Mech.* **22**, 385–400, 1965.
31. McLaughlin, J. B., Inertial Migration of a Small Sphere in Linear Shear flows, *J. Fluid Mech.* **224**, 262–274, 1991.
32. Dandy, D. S., and Dwyer, H. A., A Sphere in Shear Flow at Finite Reynolds Number: Effect of Shear on Particle, Lift, Drag and Heat Transfer, *J. Fluid Mech.* **216**, 381–410, 1990.
33. Chang, E. J., Accelerated Motion of Rigid Spheres in Unsteady Flows at Low to Moderate Reynolds Numbers, Ph.D. Thesis, Brown Univ., Providence, RI, 1992.
34. Chang, E. J., and Maxey, M. R., Unsteady Flow About a Sphere at Low to Moderate Reynolds Numbers. Part I. Oscillatory Motion, *J. Fluid Mech.* **277**, 347–379, 1994.
35. Odar, F., Forces on a Sphere Accelerating in a Viscous Fluid, Ph.D. Thesis, Northwestern Univ., Evanston, IL, 1962.
36. Odar, F., and Hamilton, W. S., Forces on a Sphere Accelerating in a Viscous Fluid, *J. Fluid Mech.* **18**, 302–314, 1964.
37. Reeks, M. W., On the Dispersion of Small Particles Suspended in an Isotropic Turbulent Fluid, *J. Fluid Mech.* **83**, 529–546, 1977.
38. Csanady, G. T., Turbulent Diffusion of Heavy Particles in the Atmosphere, *J. Atmos. Sci.* **20**, 201–208, 1963.
39. Gore, R. A., and Crowe, C. T., Effect of Particle Size on Modulating Turbulent Intensity, *Int. J. Multiphase Flow* **15**, 279–285, 1989.
40. Gore, R. A., and Crowe, C. T., Modulation of Turbulence by a Dispersed Phase, *ASM. J. Fluid Eng.* **113**, 304–307, 1991.
41. Wang, L.-P., and Maxey, M. R., Settling Velocity and Concentration Distribution of Heavy Particles in Homogeneous Isotropic Turbulence, *J. Fluid Mech.* **256**, 27–68, 1993.
42. Maxey, M. R., The Gravitational Settling of Aerosol Particles in Homogeneous Turbulence and Random Flow Fields, *J. Fluid Mech.* **174**, 441–465, 1987.
43. Wang, L.-P., and Maxey, M. R., The Motion of Microbubbles in a Forced Isotropic and Homogeneous Turbulence, *Appl. Sci. Res.* **51**, 291–296, 1993.
44. Wang, L.-P., and Maxey, M. R., Interactions of Heavy Particles with Small-scale Flow Structures in Homogeneous, Isotropic Turbulence, Fifth Int. Symp. on Gas–Solid Flow, ASME Fluids Eng. Conf., Washington, DC, June 1993.
45. Maxey, M. R., Chang, E. J., and Wang, L.-P., Simulation of Interactions Between Microbubbles and Turbulent Flow, *Appl. Mech. Rev.* **47**, S70–S74, 1994.
46. Kiger, K. T., and Lasheras, J. C., Evolution of a Dilute Spray During Vortex Pairing Within a Turbulent Shear Layer, Presented at 12th U.S. Natl. Congr. Appl. Mech., Seattle, WA, June 27–July 1, 1994.
47. Lazaro, B. J., and Lasheras, J. C., Particle Dispersion in the Developing Free Shear Layer. Part 1. Unforced Flow, *J. Fluid Mech.* **235**, 143–178, 1992.
48. Lazaro, B. J., and Lasheras, J. C., Particle Dispersion in the Developing Free Shear Layer. Part 2. Forced Flow, *J. Fluid Mech.* **235**, 179–221, 1992.

Received March 2, 1994; revised October 5, 1995